On the Use of Artificial Neural Networks for Biomedical Applications

Chapter · January 2012

DOI: 10.1007/978-3-642-33941-7-40

2 authors:

Maria Da Graça Ruano
Universidade do Algarve
126 PUBLICATIONS **733** CITATIONS
SEE PROFILE

Antonio Ruano
Universidade do Algarve
268 PUBLICATIONS **3,682** CITATIONS
SEE PROFILE

On the Use of Artificial Neural Networks for Biomedical Applications

Maria Graça Ruano[1] and António E. Ruano[2]

[1] CISUC, University of Coimbra, and the University of Algarve, Portugal
mruano@ualg.pt
[2] Centre for Intelligent Systems,
IDMEC, IST and the University of Algarve, Portugal
aruano@ualg.pt

Abstract. Artificial Neural Networks (ANN) are being extensively used in many application areas due to their ability to learn and generalize from data, similarly to a human reaction. This paper reports the use of ANN as a classifier, dynamic model, and diagnosis tool. The examples presented include blood flow emboli classification based on transcranial ultrasound signals, tissue temperature modeling based on imaging transducer's raw data and identification of ischemic cerebral vascular accident areas based on computer tomography images. In all case studies the performance of ANN proves to produce very accurate results, encouraging the more frequent use of these computational intelligent techniques on medical applications.

Keywords: biomedical applications, artificial neural networks.

1 Introduction

In this paper we report the use of ANN in practical biomedical applications. ANNs date back to 1940 and since then they have been used in many research and development applications. Since biomedical engineering involves interdisciplinary areas, the development of clinical applications requires the use of state-of-art technology such as the artificial neural networks (ANNs).

The efficiency of ANNs depends on the matching of the type of network and the addressed problem and the suitability of the ANNs parameters as representative of the target goal.

As examples of successful combinations between ANNs types and medical applications we expose the following case-studies: blood flow emboli classification based on transcranial ultrasound signals, tissue temperature modeling based on imaging transducer's raw data and identification of ischemic cerebral vascular accident areas based on computer tomography images.

Short description of the problems to be solved, calling attention to particularities of each case-study is presented in the next section. Summary versions of the NN's employed are included and finally the results are presented.

V.E. Balas et al. (Eds.): Soft Computing Applications, AISC 195, pp. 433–451.
springerlink.com

2 Case-Studies

We focus on three types of problems: classification of different type of emboli within blood flow signals, a diagnostic tool based on CT images and tissue temperature non-invasive estimation.

Transcranial Doppler (TCD) ultrasound is an established method for detecting emboli in the cerebral circulation. The differentiation between gaseous and particulate emboli in cerebral blood flow is clinically relevant because different therapeutics should be administrated. The application of TCD in clinical practice relies on human expertise to detect and classify events in the generated signals, constituting a fastidious and time consuming task. The existence of alternative and preferably software-based automatic detection led to the investigation of the applicability of ANN in emboli classification.

At the time this research was held, several signal processing methods had been proposed in literature, essentially based on signal processing methodologies. To be mentioned, the application of the Wigner distribution [1] where the separation between types of emboli was based on measurements of the sample volume length (given by the product of embolic duration and velocity) against the physical length over which the signal could be detected. Blood velocity measurements are by themselves difficult to obtain with accuracy due to flow velocity dependence on many parameters inducing as so a non-stationary nature. Alternatively researchers applied time-frequency and time-scale based matched-filters like the Wavelet Transform (WT) [2-3] proving that WT were better suited for processing this type of signals. To be also referred that Kemény et al. [4] reported the detection and classification of cerebral embolic signals from TCD systems using ANNs after pre-processing the signals with the help of Fourier Transforms. Since the embolic signals present a similar shape to the Morlet wavelet (see Fig. 1), a wavelet neural seemed appropriate for identifying emboli within the blood flow signal and then we tested the classification of the type of emboli using a Multi-Layer Perceptron (MLP) NN [5].

Later a radial basis function (RBF) ANN was also assessed to distinguish among solid emboli, liquid emboli, or artifacts, using as indicators a ratio between signal powers and emboli duration [6].

In what considers the diagnosis tool application one should recall that the ischemic cerebral vascular accident (ICVA) is one of the major causes of death in the developed countries. The early diagnosis of this pathology is fundamental to minimize the consequences of this disease. ICVA is typically diagnosed through Computerized Tomography (CT) by identification of hemorrhages (characterized by a high density (white) image and usually occupying a round-spaced area), or an infarct (characterized as a low density (dark) image and occupying a vascular territory with some swelling) [7]. CT provides images from inside the human body with anatomic detail, being able of generating images of the human body in different planes [8] through image processing workstations. This facility has the disadvantage of producing a large increase in the number of images to be analyzed in terms of their content on anatomic information, besides the fact that each patient exhibits several individual images to be examined. Detailed examinations of each image become a very time consuming task for the radiologists therefore the existence of a computational facility capable of

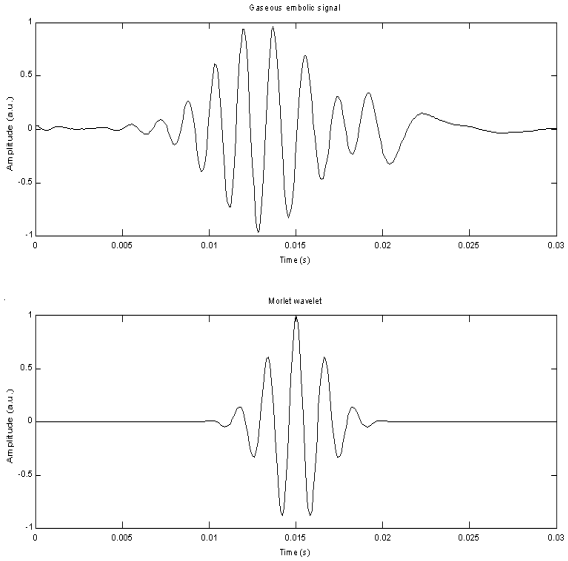

Fig. 1. The shape of an embolic signal (a)) is similar to a Morlet wavelet (b)) (a. u. = arbitrary units)

assisting the clinician on the task of ICVAs identification would be of great help. In this sense Radial Basis Function Neural Networks (RBFNN) were applied in images of encephalon acquired by CT scan to research their ability to identify ICVA areas.

The last case-study to be reported in this paper is concerned with tissue temperature estimation. Ultrasound is daily used in medicine for diagnosis and its applicability in therapy has been increasing within the last two decades. Ultrasound thermal therapies are being deeply researched towards the controlled spatial and temporal application of heat to delimited regions aiming at cancer tissue treatment [9]. Precise control of ultrasound instrumentation requires knowledge of accurate models capable of determining non-invasively the temperature of the tissues under treatment in both space and time variables [10]. Since *in-loco* determination of temperature in real patients is not desirable, several experiments using tissue mimicking materials, the so called phantoms, have been performed. The phantoms vary according to their chemical composition, mimicking single type of tissue or, the more complex and realistic ones, mimicking structures composed of different tissues [11]. Tissue reaction to heat depends on several variables, namely the velocity of propagation of sound on that particular tissue, the tissue rate of absorption and attenuation, the way the ultrasound waves are reflected and refracted when crossing two different media. So, realistic models of ultrasound induced temperature are expected to be nonlinear due to the combination of so many variables. The gold standard error for temperature estimation on tissues is considered to be 0.5ºC/cm^3 [10], value obtained by magnetic resonance imaging. Typical methods of non-invasive thermometer make use of backscattered ultrasound signals in different approaches: those who track the echo-shifts produced by changes in sound velocity and medium expansion/compression, the ones which are

based on the measurement of the attenuation coefficient, and those measuring the change on backscattered energy [10].

Among the ultrasound temperature dependent features pointed out for estimation under hyperthermia range, we concentrate on temporal echo-shifts. We started to analyze the behavior of temperature induced by ultrasound in homogenous medium phantoms and then we developed to heterogeneous phantoms. Radial basis functions NN were tested in comparison with autoregressive with exogenous inputs (ARX) models [12]. The NN promising results lead to the application of RBFNNs with best fitted NN parameters selected by a Multi-Objective Genetic Algorithm (MOGA) to increasingly complex data models [13-15].

3 Methods

To enable the reader with a more clear understanding of the particularities of each case-study in relation with the type of ANN methodology employed, each method will be independently presented.

3.1 WNN for Emboli Classification

The gaseous embolic signals present great dynamic range while solid emboli are normally of lower amplitude. When these signals are recorded from TCD systems with two channels (as the case of signals employed in this study) the channels are set to have 40dB attenuation between them to accommodate these differences. Solid and gaseous emboli are collected from the first and second channels respectively. In our study we employed 200 files (both channels), each containing 30000 samples of 2.4s of Doppler signal. A group of experts classified the signals so we were sure that each signal contained at least one event (solid or gaseous emboli). Manual analysis of the events enabled selection and recording of 1000 sample signals correspondent to 80ms of Doppler signals, including 137 gaseous emboli, 119 solid emboli and 150 normal flow events.

Primarily all signals from the sample data set were approximated using a wavelet NN (WNN) whose network nodes used a Morlet wavelet. The WNN was composed of a number of wavelet nodes (10), each described by three parameters: the dilation of the wavelet function (d), the translation (t) and the linear weight (w). The output of such a network is given by [16]

$$g(x) = \sum_{i=1}^{10} w_i \cdot \psi(d_i(x - t_i)) \tag{1}$$

where x represents time and ψ is the wavelet function used in the WNN, defined by:

$$\psi(x) = \cos(2\pi x) \cdot \exp\left(-x^2/2\right) \tag{2}$$

The WNN required an initialization phase where the desired resolution levels (dilations) are selected using a regular wavelet lattice. Then, from this data, the desired number of wavelets was selected using the algorithm of stepwise selection by orthogonalization [17].

The training of the WNN is based on a set of input/output pairs $\{x, f(x)\}$ where $f(x)$ is the function to be approximated. After the initialization, the network was trained by a Gauss-Newton procedure [17]. To perform this approximation, the normalized square root of the mean square error (NSRMSE), given by (3), was used to verify the quality of the approximation.

$$NSRMSE = \sqrt{mse} \Big/ \sigma_y \tag{3}$$

In (3) above, $mse = \sum_{n=1}^{N} (y - g)^2 \Big/ N$ is the mean square error of the approximation, with y the value of the function, g the approximation, N the dimension of y, and σ_y the standard deviation of y.

Then two NNs were trained with the parameters obtained from the approximation part. One network learned to distinguish between normal flow signals and embolic signals while the other learned to separate gaseous from solid embolic signals. Supervised learning with the same learning algorithm was used in both networks: a Multi-Layer Perceptron (MLP) implemented in Matlab and trained by a version of the Levenberg-Marquardt algorithm, which explicitly separates the role of the linear and nonlinear network parameters [18].

3.2 RBFNN for Emboli Classification

For the same type of embolic data another ANN approach has been tried, the RBFNN [19]. A RBFNN consists of three fully connected layers. The first is the input layer connecting the source nodes to the hidden layer of the network. The second is a hidden layer of sufficient dimension for the problem at hand which applies a non-linear transformation to the input space generating a (usually) higher-dimensional hidden-units space. The third and last layer applies a linear transformation from the hidden-units space to the output space.

The topology of a RBF neural network is shown in figure 1. Its output is given by

$$f(\mathbf{x}) = \alpha_0 + \sum_{i=1}^{n} \omega_i \varphi_i (\mathbf{x}, \mathbf{c}_i, \sigma_i), \tag{4}$$

where n is the number of neurons, α_0 is a bias term and ω_i are weights for the output linear combiner. The function used in the RBF hidden layer cells is usually a Gaussian function of the form:

$$\varphi(\mathbf{x}, \mathbf{c}_i, \sigma_i) = e^{-\frac{\|\mathbf{x}-\mathbf{c}_i\|^2}{2\sigma_i^2}} \tag{5}$$

$\mathbf{c_i}$ and σ_i are, respectively, the centre locations and spreads of the Gaussian function φ_i and $\mathbf{x}$ is the input pattern.

TCD exams have also been used. In this particular study six files of TCD exams (each file with 1880000 points) were preprocessed before used in the training and testing phases.

Primarily data was divided into 128 points segments using a Hanning window and 50% overlap was employed during spectrograms' calculations. Then, computation of clinically relevant characteristic, the embolic power by segment (EPS) and the embolic temporal duration [20], this is, the time interval where the embolic signal amplitude is 10dB above the scattered blood flow signals, were performed. These data information was used to calculate the ANN target output. To reflect the subjective nature of the specialists' decisions emboli duration and EPS were classified according to the range of values specified in Table 1.

Table 1. Emboli classification used in creation of the target output of the RBFNN approach

Parameters	Solid emboli	Gaseous emboli
Duration	(5.76 to 27.52)ms	(39.12 to 65.04)ms
EPS	(16.3 to 24.9)dB	(34.5 to 39.4)dB

The convention used in the assignment of values to the target output was the following:

- If EPS and Embolic Duration do not lie in the intervals presented in Tab. 1 then the target output should be 0, and the signal is classified as an artifact.
- If EPS $\in$ [16*:*3*dB;* 24*:*9*dB*] and Duration $\in$ [5*:*76*ms;* 27*:*52*ms*] then the signal is classified as a solid emboli, and the target output is assigned with the value 1.
- If EPS $\in$ [34*:*5*dB;* 39*:*4*dB*] and Duration $\in$ [39*:*12*ms;* 65*:*04*ms*] then the signal is classified as a gaseous emboli, and the target output is assigned with the value 2.

After these calculi the data sets to be used in the training and test phases were created as a concatenation of the signal characteristics and the target outputs to avoid patient's dependency. To optimize the training of the RBFNN and reduce the training time the concatenated data was normalized, shuffled and non-relevant data was eliminated to optimize the RBFNN's training. With this procedure the 60000 patterns available at the beginning of this study were reduced to 134 patterns, where 90 patterns were used during training and 44 patterns were left for the testing phase.

The training of the NNs was performed by the Levenberg-Marquardt (LM) algorithm using preprocessed data. The LM is a completely supervised learning algorithm. This means that given the initial values of the parameters, the training algorithm iteratively, having as objective the minimization of a cost function, can determine the "optimum" value of the network parameters (linear weights, centers, and spreads). In this paper the initial values of the parameters were determined using the optimal k-means algorithm (OAKM) [21].

Using the referred algorithm, 19 networks were trained using a different number of neurons in the hidden layer. The number of neurons varied between 2 and 20, and it was imposed 3 as the number of correct digits in the objective function. With this accuracy an acceptable quality for the trained networks was achieved, without originating sub-modulated networks.

3.3 ICVA Diagnosis Tool

A RBFNN model has also been employed in this case-study. The training method [22] employed consisted of two steps: primarily, an unsupervised procedure known as the *optimal adaptive k-means clustering* (OAKM) algorithm [21] was used to compute the initial centre locations, and a simple method [23] is adopted to determine the initial spreads. The second step uses a supervised training method that employs the Levenberg-Maquardt (LM) [24] algorithm to further optimize the non-linear parameters ($\mathbf{c}_i$, σ_i - see equations 4 and 5) of the network. In each training iteration the output linear weights, α_i, are computed as a least-squares solution. The method reflects the non-linear/linear topology of the RBF neural network. The termination criterion used to stop the training procedure is commonly used in non-linear optimization problems. It depends on one parameter related to the number of correct figures in the objective function and uses also the gradient and parameter vectors to assess convergence of the parameter values [22]. When all the stopping conditions are met the training stage is ended and the parameters of the network are stored for latter usage.

A group of images from 25 encephalon exams with previous ICVA diagnosis were used. The images employed were all acquired by means of the same CT equipment, respecting the protocol for encephalon study (5/5-10/10mm), and archived in DICOM format. In the laboratory they were converted into the Portable Network Graphics (PNG) format with 256 tones of grey, respecting the original image size (512x512). HUV values for each series of the study had been respected, to ease the process of analysis of the NN. All the points of interest were automatically masked in order to remove the white parts corresponding to bone or other regions not meant to be classified. Some small regions of interest were manually labeled as 1 when ischemic and 0 when normal. From each image and the pixels within the chosen regions, a set of features was extracted. The features were chosen to reflect the image statistics and those related to the context of the pixels of interest, the presence of structures having sharp edges and the position within the image. Altogether, these features form one possible data set suitable to train a RBFNN pixel classifier.

3.4 Dynamic Model for Tissue Temperature Estimation

Our research in temperature modeling of human tissue subjected to ultrasound for therapeutic purposes was based on data collected from artificial tissues, the so called phantoms. Homogeneous and heterogeneous phantoms under different ultrasound devices operating conditions have been tested. The laboratorial experimental setup is based on a typical structure shown in Fig. 2.

The phantom is heated by a therapeutic transducer while immersed in a degassed water tank in order to discard abrupt room temperature changes and to improve the coupling between the transducers and the medium. The medium is heated by a commercial therapeutic ultrasound transducer (TUS). The TUS transducer has an effective radiation area of 3.5 cm^2, and works in continuous mode at 1or 3 MHz. Different intensities are available at user's definition. The RF-lines are collected using an imaging ultrasound (IUS) transducer working in pulse-echo mode, driven by a pulser/receiver. The pulser/receiver sends the analog RF-lines to an oscilloscope which

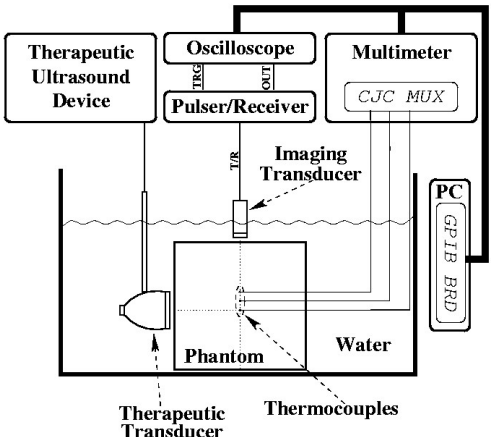

Fig. 2. Basic ultrasound experimental setup

digitalizes them at 50 MHz. The digitalized RF-lines are then sent to a personal computer (PC) via a GPIB bus. The effective temperature of the medium is measured by a certain number of thermocouples placed at a specific distance from the TUS transducer face in its radial line and aligned with the IUS. In the case of figure 2, three thermocouples are shown. The thermocouples are connected to a digital multimeter. The temperature values are transferred to the PC via the GPIB bus. At each 10s a RF-line is collected, as well as the thermocouples' temperature values. The medium is heated for a pre-defined period of time, and typically allowed to cool for an equal period.

The study of the temperature evolution is to be performed independently at the points defined by each thermocouple location, then each echo was isolated using a rectangular window, and the echo-shifts computed for each one. The echo-shifts were computed using an algorithm that directly evaluates continuous time echo shift (TES) from sample data. This method constructs a splinebased, piecewise continuous representation of a reference signal (in this case the echoes in the first RF-line), then finds the minimum of the sum of the squared errors between the reference and the delayed signals to determine their relative time-shift [25]. Also past temperatures of the medium were considered as important information on the estimation procedure.

Considering the huge amount of data available the selection of the appropriate number of neurons that produces the smallest NN error, the identification of the most relevant input variables to fit the model, the important lags of those variables are decisions difficult to be taken. To help on this task the best fitted RBF structures were selected by MOGA [26]. The MOGA is an evolutionary computing approach based on the natural evolution, and designed to minimize (or maximize) a number of problem-dependent objectives. Having in mind the attainment of good and also feasible solutions for a given application the objectives are defined as goals to meet. Each goal can have an associated priority which describes the relative importance of the related goal for the problem solution. At the end of a MOGA run a set of preferable individuals (solutions) are attained which are the ones that fulfill or almost fulfill the a-priory defined goals.

In almost all our case studies the MOGA search space was delimited by defining the possible number of neurons in the hidden layer, the possible number of inputs, and the maximum lag for TES and the changes in temperature signals (ΔT). The number of neurons and the maximum number of inputs was, in general, defined as a number in the interval [8, 20] and 25, respectively. These values were selected after several runs considering other parameter's arrangements.

Several models have been implemented, considering variations in experimental conditions. We started by estimating temperature in a single spatial location of a glycerine (homogeneous medium) tank, testing three TUS intensities (1 Watt/cm^2, 1.5 Watt/ cm^2, and 2 Watt/ cm^2)[12]. Experiences took 110 minutes where the first 60min correspond to medium heating and in the remaining 50min data was also collected to observe the cooling stage of the experiment. The RBFNN input variables in this preliminary study considered the fundamental component of the intensity spectrum and the measured temperature. The number of model inputs was allowed in the interval [2,30], while the possible number of neurons was accepted to be in the interval [2,15].

The RBFNN single point temperature estimation was then compared with the results of an ARX model defined by the equation

$$y[t] + a_1 y[t-1] + \cdots + a_{na} y[t-na] = b_1 u[t-nk] + \cdots + b_{nb} u[t-nk-nb+1] \quad (6)$$

Where the actual output y[t] is related with a finite number of values of the output y[t-k] and of the input x[t-k]. The structure of the model is defined by the number of poles (na), the number of zeros (nb-1) and the time delay of the system (nk). The model coefficients $\{a_i\}_{i=1}^{na}$and $\{b_i\}_{j=1}^{nb}$were determined using the least squares strategy.

Later we increased to three the spatial points where temperature was to be estimated as seen in Fig. 3. In terms of the model, the position along the axis was considered as another input. The phantom, still a homogeneous medium, was prepared to mimic human muscle by mixing (in % weight): 86.5% of degassed water, 11% of glycerin, and 2.5% of agar-agar. Data has been collected during 35minutes where the first 5 minutes enabled representation of resting conditions of the medium, the next 15min correspond to heating phase and the remaining time is representative of the cooling stage. The computed echo-shifts and the measured temperature values were filtered and normalized to values between -0.5 and 0.5. The filtration was performed to reduce the computational and measurement noise, and the normalization was computed to discard the difference in scale between the echo-shifts signals and the measured temperature signals. Afterwards the normalized and filtered *TES* and *ΔT* were arranged in separated files, according to the related intensity and spatial point (P1, P2, or P3 in Fig. 3), and applied in the RBFNN construction [13].

The neural network parameters were found using the Levenberg Marquardt (LM) algorithm and the least-squares strategy. At each MOGA iteration the performance of each NN is accessed in order to extract the problem-dependent objectives under minimization, this is, the model errors, validity tests, linear weight norm, and computational complexity.

Aiming at a more detailed analysis, the number of spatial points inside the tissue phantom have then been increased to five (with relative positions as in Fig. 3 but spaced among them by 5mm) and a new TUS intensity (0.5W/cm^2) was tested [14].

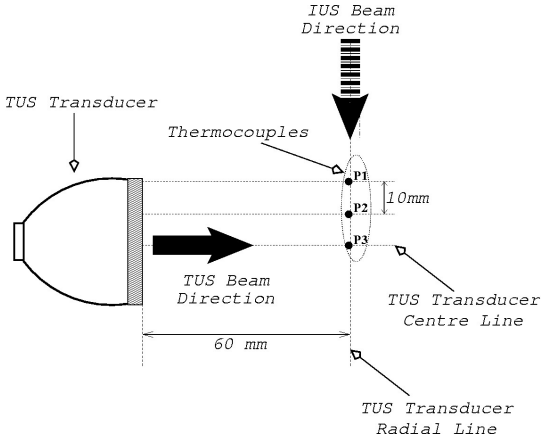

Fig. 3. Thermocouples disposition in relation to the therapeutic (TUS) and imaging (IUS) transducers denoting spatial point locations for temperature estimation

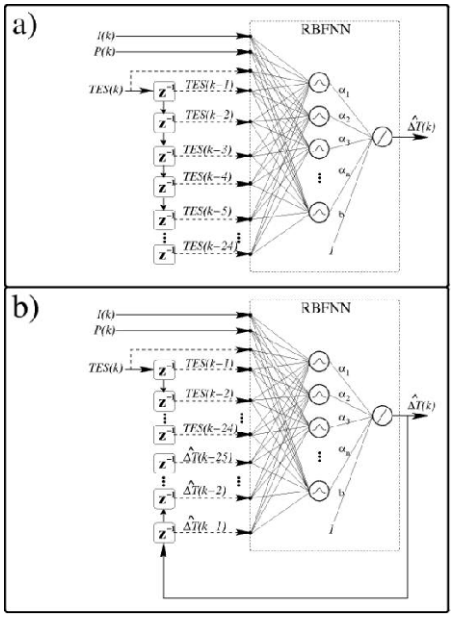

Fig. 4. Generic RBFNN structures applied. (a) non-regressive and (b) regressive.

Also the temperature of the degassed water tank containing the phantom was maintained at approximately 22 ºC, by using a 75-W aquarium heater. The NN input variables considered up to 25 past lags of ΔT and *TES*. With these data two three-layered RBFNN structures were tested: a generic non-regressive structure considering only the past lags of *TES* as inputs, as presented in Fig. 4a; and, a regressive structure where both the ΔT and the *TES* past values were considered, as shown in

Fig. 4b. In both structures two additional inputs were considered to discriminate the intensity and spatial point under estimation. Four MOGA runs of 200 generations were performed for both structure types. To test the spatial generalization capacity of the best obtained models, training and structure selection considered only estimations in three of the five spatial points (extremes and middle points). Then, at the final step, the validation set contained data from all the five points, implementing a real generalization assessment procedure.

Maintaining the recursive RBFNN structure (Fig. 4 (b)) the research developed to estimate temperature on a three-layered non homogeneous phantom (Fig. 5) with attenuation and speed-of-sound similar to in vivo muscle [15]. Besides using a more complex phantom, the number of intensity levels applied was increased (0.3, 0.5, 0.7, 1.0, 1.3, 1.5, 1.7, and 2.0W/cm^2). Since the influence of the ultrasound operating conditions were to be tested in this study, the division of the available data set considered for training and testing data sub-sets where only four intensity levels were considered (0.5, 1.0, 1.5, and 2.0W/cm^2). Validation was performed on all range of intensities evaluated experimentally.

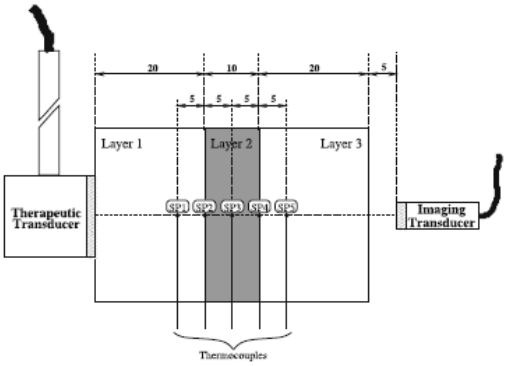

Fig. 5. Transducers (located face to face) and thermocouples location inside the heterogeneous phantom (all length units are in mm)

4 Experimental Data and Results

Following the same policy as in the previous section, the experimental data available, how it was used as input to the NNs and the correspondent results will be exposed separately for each case study.

4.1 Classification of Emboli

As previously stated in this case-study, from the 200 data files recorded from a TCD system, where each file contained at least one gaseous or solid embolic event (already classified by a group of experts) were manually selected and recorded as 1000-sample signals (corresponding to 80 ms blood flow signals). For each signal, the network parameters were adapted for 10 epochs to minimize the error between the original

signal and the output of the WNN, using the Gauss-Newton method. The wavelet parameters that best fitted each signal were saved to be used during the classification stage. The performance of the approximation of the Gauss-Newton procedure was assessed by the normalized square root of the mean square error (NSRMSE) whose values ranged from 0.07 to 0.73 to accomplish the fact that the surrounding signal presented amplitudes of the order of the event itself.

Next the MLP was implemented with 30 inputs, one hidden layer with 3 nodes and one output layer with 2 nodes.

The first NN was trained to classify signals as normal flow or embolic. This target and the training set (composed of the 170 examples of embolic signals, gaseous and solid, plus the 100 examples of normal flow signals) were presented to the NN. Training was repeated 100 times with different initial conditions and the best results chosen.

The results obtained for this first NN, as percentages of correctly classified signals, are shown in Table 2.

Table 2. Classification results for embolic and normal signals

	Training phase	Test phase
Embolic signals	98.8	91.9
Normal signals	97.0	96.0

The second NN was trained to classify embolic signals in gaseous or solid emboli. Training of this network (also 100 times repeated under different initial conditions) was done with 170 example signals in the training set and 86 in the test set. Table 3 shows the percentages of correct classifications obtained.

Table 3. Classification results of wnn for gaseous and solid emboli

	Training phase	Test phase
Gaseous emboli	91.1	91.5
Solid emboli	98.8	97.7

When the embolic data was assessed by the RBFNN, all networks were evaluated having in mind the decision levels described in Table 1. Table 4 shows the performance of a network with 2, 6 and 18 neurons. The network employing 6 neurons was the best performing one, presenting approximately 88% of success.

Table 4. RBFNN performance

Neurons	Training success	Testing success
2	71.7	62.5
6	100	87.5
18	100	12.5

Comparing these results with the WNN methodology and considering the success of RBFNN networks on other applications one should conclude that, besides the very good performance obtained there is still room for exploring other methods of pre-processing the data to be used in training and testing phases and to investigate the incorporation of more entries in the network.

4.2 ICVA Diagnosis Tool

When computing the features, only the points lying within the mask are considered. The left image in Fig. 6 shows an example of a masked exam. Bone areas and other artifacts are all shown in black. The right image shows the complete exam.

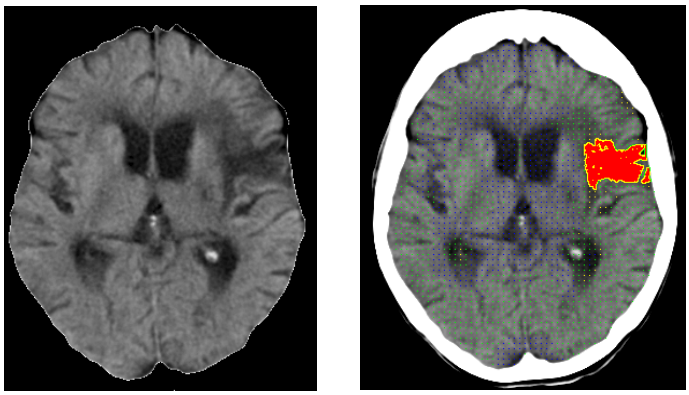

Fig. 6. Image from patient P06, exam 01. Left: masked image submitted to the network; right: Output from the classifier.

From a set of 25, exams were randomly collected from 2 patients (P03, P06). P06 contributed with 10 points to the training set, while 2 points were taken from PO3 (see Table 5).

Table 5. Points used to train the RBF neural network

	Image 02		Image 03		Image 05		total
	Positive	Negative	Positive	Negative	Positive	Negative	
P06	2	4	1	1	2	-	10
P03	-	-	-	-	1	1	2

A first experiment considered NNs trained with 3 parameters. Different number of trials were run varying the number of neurons in the NN and performances were recorded. The performance was evaluated by the error measured between the desired classification and the network output. For the best neural network achieved, all images from the patients sample were submitted to the classifier and the results were analyzed and compared to the radiologist report.

In operation, to avoid so heavy computation burden, instead of feeding all the pixels to the network, only those in a sub-sample grid were submitted. When one of these was reported as corresponding to pathology, all its neighbors were also submitted to the network. The process is repeated in a recursive way until no neighbor pixels are reported as pathological. The whole process was repeated by removing or adding features to the network input and by varying the number of neurons for each input configuration. After a number of trials the results were significantly improved by a 5 neurons neural network having 6 features.

The output images of the classifier are marked with different colors depending on the neural network output for each tested pixel. The following color code was used regarding the network output:

- [0.0, 0.2[– clear absence of pathology (blue);
- [0.2, 0.5[– absence of pathology (green);
- [0.5, 0.75[– marginal positive (yellow);
- [0.75, 1.0] – pathology (red).

As it can be seen in the right image of Fig. 6 the NN located the ischemic areas and marked them as described in medical report. In Fig. 6 it can be seen that the NN delimits the ischemic injury, marking the border of the injury (in yellow) with satisfactory accuracy. In possible areas of error such as sharp ridges and hypertrophic ventricles, the NN accuracy is confirmed by the mapping of colors.

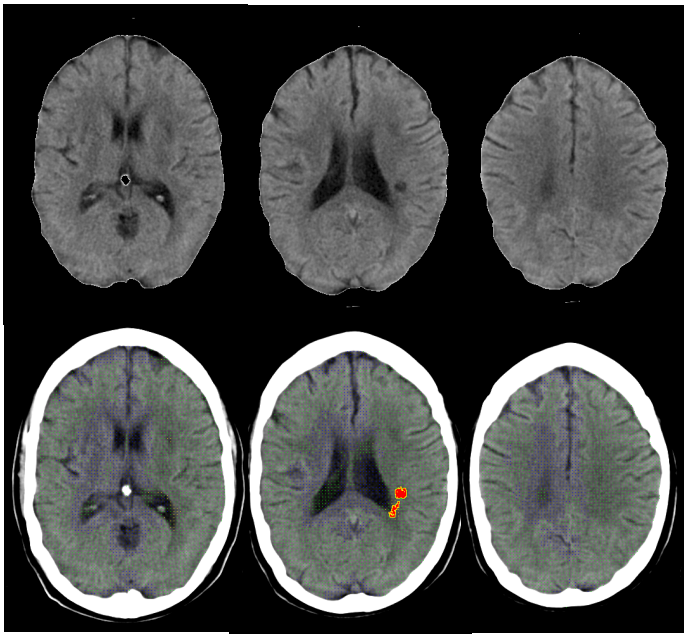

Fig. 7. Images from patient P19. Top: input images; bottom: output from the classifier.

Fig. 7 presents results regarding patient P19. In these images a small lacuna infarct is visible and correctly marked by the NN. This type of injury, usually visible only in one cut because of the reduced dimensions (perhaps in two according to the thickness of the cut), was also detected by the NN. The classifier demonstrated capacity of generalization when marking this zone of ischemia, considering that none of the training images included a similar injury. On the other hand a small error in the posterior horn of the left lateral ventricle is present, when the results of the NN are compared to the radiologist report.

The results obtained with this study [27-28] achieved around eighty percent of success. Besides the need for more tuning of the methods one can conclude that the neural network approaches can offer to the area of image based medical diagnose a great value, minimizing the time to report and therefore providing a faster treatment.

4.3 Dynamic Model for Tissue Temperature Estimation

Our preliminary NN temperature modeling considered 11 models (identified by MOGA) with different combinations of fundamental components of the spectrum and ΔT lags. The best ARX structure was computed considering a scanning of 48 lags (na = 1,...,48, nb = 1,...,48) for each variable, and a null delay for the inputs (nk =0). The ARX model presented a RMSE in the validation set of 0.0253, and a maximum absolute error of 2.1 ºC while the best fitted RBFNN model presented a maximum absolute error of less than 0.2ºC encouraging research of RBFNNs for temperature estimation. A graphical representation of the comparative behavior of these methods can be observed in Fig. 8.

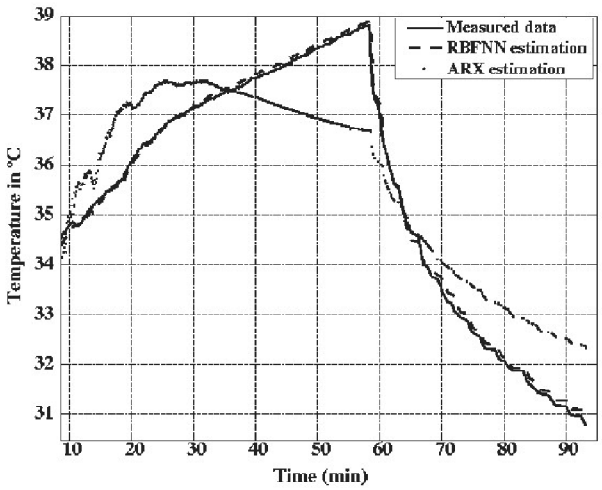

Fig. 8. Estimated outputs of RBFNN and ARX models in comparison with a measured output when a homogeneous phantom is employed

When we improved the tissue mimicking properties of the phantom in use (although still as a homogeneous medium) and investigated the behavior of three different TUS intensities, the best RBFNN presented a maximum absolute error of 0.45 ºC, which was inferior to the value required for hyperthermia/diathermia purposes. This best model was validated for all the possible situations, i.e. at all the intensities and points (positions) studied. The estimated temperature curves followed the curves of the measured temperature both at heating and the cooling phases of the experiment denoting a high generalization capacity of the model.

The regressive and non- regressive RBFNN structures, tested for five spatial points and four TUS intensities proved that the regressive approach presented less temperature estimation errors (see Fig. 9). In fact, considering the trained (extreme and middle spatial points) and untrained (other two points) and all the best models, a maximum absolute error of 0.5ºC and 4.4ºC was respectively obtained for the non-regressive structure. The best model (18 neurons and 9 inputs, reaching a number of 199 parameters) attained a mean maximum error of 0.8ºC. On the other hand, the best performed regressive RBFNN structure presented a maximum absolute error of 0.4ºC for the trained spatial points and 0.5ºC for the untrained ones. This regressive model

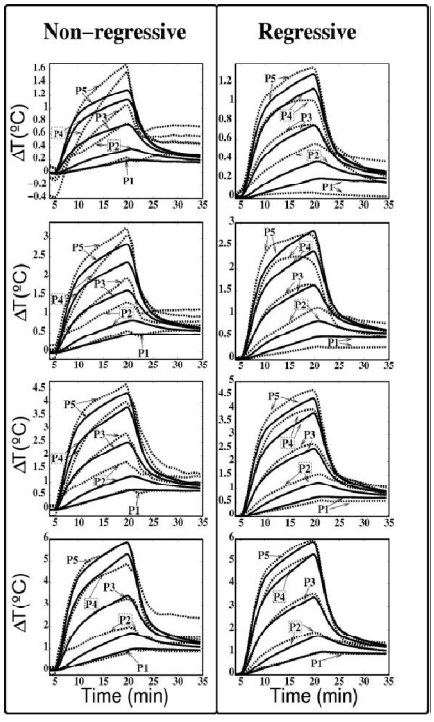

Fig. 9. Estimated versus measured temperature waveforms by the best regressive and non-regressive RBFNN estimators

presented 10 neurons and 13 inputs reaching a number of 151 parameters. It is worth mentioning that the advantage of using the non- regressive model would not to need to know the initial temperature of the medium, which might be considered a valuable issue in terms of clinical application of these estimators.

When a three-layered media phantom was experimented under eight TUS intensities, the best achieved model respected the gold standard 0.5ºC maximum error, independently of the intensity and the spatial position considered, which was a novel achievement. During this study models were trained and selected to estimate temperature at four intensities, then during the validation phase, the best fitted models were analyzed in data collected at the eight intensities. Therefore, once more the generalization ability of RBFNN was proved. More detailed description of RBFNN modeling of tissue temperature estimation could be find in [29-33].

5 Conclusions

This paper reports several biomedical cases and how they have been dealt to achieve parameters' estimation using NNs in particular RBFNNs. From classification of emboli based on transcranial Doppler ultrasound blood flow signals, to the design of a diagnostic tool for ICVA identification, and finally the temperature estimation on ultrasound induced hyperthermia making use of simple to more realistic phantoms, we described the methods employed and detailed how data was used as inputs of the NNs. In all cases, very high performance was achieved proving that ANN should be used more frequently and included on medical applications.

References

1. Fan, L., Evans, D.H.: Extracting instantaneous mean frequency information from Doppler signals using the Wigner distribution function. Ultrasound Med. Biology 20, 429–443 (1994)
2. Devuyst, G., Vesin, J.-M., Despland, P.-A., Bogousslavsky, J.: The matching pursuit: a new method of characterizing microembolic signals? Ultrasound Med. Biology 26, 1051–1056 (2000)
3. Matos, S., Leiria, A.I., Ruano, M.G.: Blood flow parameters evaluation using wavelet transforms. World Congress on Medical Physics and Biomedical Engineering, 4235-52803.pdf, CD-ROM, Chicago, USA (2000)
4. Kemény, V., Droste, D.W., Hermes, S., Nabavi, D.G., Schulte-Altedorneburg, G., Siebler, M., Ringelstein, B.: Automatic embolus detection by a neural network. Stroke 30, 807–810 (1999)
5. Sérgio Matos, A.E., Ruano, M., Ruano, G., Evans, D.H.: Neural network classification of cerebral embolic signals. In: 23rd Annual International Conference of the IEEE Engineering in Medicine and Biology Society, paper 1123, track 4.3, CDROM, Instambul, Turkey (2001)
6. Teixeira, C.A., Graça Ruano, M., Ruano, A.E.: Emboli classification using RBF neural networks. In: Proceedings of CONTROLO 2004, Faro, Portugal, June 7-9, pp. 630–635 (2004)

7. Wardlaw, J.: Radiology of Stroke. J. Neurol Neurosurg Psychiatry 70(suppl. I), i7–i11 (2001)
8. Robb, W.: Perspective on the First 10 Years of the CT Scanner Industry. Academic Radiology 10(7), 756–760 (2003)
9. Arthur, R.M., Straube, W.L., Trobaugh, J.W., Moros, E.G.: Noninvasive temperature estimation of hyperthermia temperatures with ultrasound. Int. J. Hyperthermia 21, 589–600 (2005)
10. Arthur, R.M., Straube, W.L., Starman, J.D., Moros, E.G.: Noninvasive temperature estimation based on the energy of backscattered ultrasound. Medical Physics 30, 1021–1029 (2005)
11. Zell, K., Sperl, J.I., Vogel, M.W., Niessner, R., Haisch, C.: Acoustical Properties of Selected Tissue Phantom Materials for Ultrasound Imaging. Physics in Medicine and Biology 52, 475–484 (2007)
12. Teixeira, C.A., Cortela, G., Gomez, H., Ruano, M.G., Ruano, A.E., Negreira, C., Pereira, W.C.A.: Temperature models of a homogeneous medium under therapeutic ultrasound. Brazilian Journal of Biomedical Engineering 20(2-3), 97–101 (2004)
13. Teixeira, C.A., Ruano, A.E., Ruano, M.G., Pereira, W.C.A., Negreira, C.: Non-invasive Temperature prediction of in-vitro therapeutic ultrasound signals using neural networks. Medical and Biological Engineering and Computing 44(1-2), 111–116 (2006)
14. Teixeira, C.A., Graça Ruano, M., Ruano, A.E., Pereira, W.C.A.: A soft-computing methodology for non-invasive time-spatial temperature estimation. IEEE Transactions on Biomedical Engineering 55(2), 572–580 (2008)
15. Teixeira, C.A., Pereira, W.C.A., Ruano, A.E., Graça Ruano, M.: On non-invasive multilayer temperature estimation using soft-computing methods. Ultrasonics 50(1), 32–43 (2010)
16. Zhang, Q., Benveniste, A.: Wavelet Networks. IEEE Trans. Neural Networks 3, 889–898 (1992)
17. Zhang, Q.: Using wavelet network in nonparametric estimation. IEEE Trans. Neural Networks 8, 227–236 (1997)
18. Ruano, A.E., Jones, D.I., Fleming, P.J.: A new formulation of the learning problem for a neural network controller. In: IEEE Conference on Decision and Control, Brighton, U.K., pp. 865–866 (1991)
19. Ferreira, P.M., Faria, E.A., Ruano, A.E.: Neural network models in greenhouse air temperature prediction. Neurocomputing 43(1-4), 51–75 (2002)
20. Matos, S., Ruano, M.G., Ruano, A.E.: Embolic signals characterization using wavelet neural networks. In: Proc. of the BioEng 2001, paper 41. University of Algarve (2001)
21. Chinrungrueng, C., Séquin, C.H.: Optimal adaptive k-means algorithm with dynamic adjustment of learning rate. IEEE Transactions on Neural Networks 6(1), 157–169 (1995)
22. Ruano, A.E., Ferreira, P.M., et al.: An Overview of Nonlinear Identification and Control with Neural Networks. In: Ruano, A.E. (ed.) Intelligent Control Using Intelligent Computational Techniques. IEE Control Series (2005)
23. Haykin, S.: Learning In Neural Networks. A Comprehensive Foundation. Prentice-Hall (1998)
24. Levenberg, K.: A Method for the Solution of Certain Problems in Least Squares. Quarterly Applied Mathematics 2, 164–168 (1944)
25. Viola, F., Walker, W.F.: A spline-based algorithm for continuous time-delay estimation using sampled data. IEEE Trans. Ultrasonics &Ferroelectric Freq. Control 52, 80–93 (2005)

26. Ferreira, P.M., Ruano, A.E., Fonseca, C.M.: Genetic assisted selection of RBF model structures for greenhouse inside air temperature prediction. In: Proc. IEEE Conference on Control Applications, Istambul, Turkey, vol. 1, 2, pp. 576–581 (2003)
27. Ribeiro, L., Ruano, A.E., Graça Ruano, M., Pedro, M.: Neural networks as-sisted diagnosis of ischemic CVA's through CT scan. In: Proceedings of the IEEE International Symposium on Intelligent Signal Processing, Spain, pp. 223–227 (2007)
28. Ribeiro, L., Ruano, A.E.B., Ruano, M.G., Ferreira, P., Várkonyi-Kóczy, A.R.: Improving the Diagnosis of Ischemic CVA's through CT Scan with Neural Networks. In: Proceedings of the 2nd IEEE International Workshop on Soft Computing Applications, Hungary, Romania (2007)
29. Teixeira, C.A., Graça Ruano, M., Pereira, W.C.A., Ruano, A.E.: Temperature modelling of an homogeneous medium using genetically selected RBF(LIC). In: Proceedings of the 16th IFAC World Congress, paper no 2387 DVD, July 4-8. Elsevier, Prague (2005)
30. Teixeira, C.A., Ruano, A.E., Graça Ruano, M., Pereira, W.C.A.: Generalization assessment of non-invasive data-driven temperature estimators from therapeutic ultrasound. Brazilian Journal of Biomedical Engineering 23(2), 143–151 (2007)
31. Teixeira, C.A., Graça Ruano, M., Ruano, A.E., Pereira, W.C.A.: Multilayered non-invasive temperature estimation from backscattered ultrasound. In: Proceedings of the Acoustics 2008, France (2008)
32. Teixeira, C.A., Pereira, W.C.A., Ruano, A.E., Graça Ruano, M.: NARX structures for non-invasive temperature estimation in non-homogeneous media. In: Proceedings of the IEEE International Symposium on Intelligent Signal Processing (WISP 2007), Spain, pp. 169–174 (2007)
33. Teixeira, C.A., Graça Ruano, M., Ruano, A.E., Pereira, W.C.A.: Neuro-genetic non-invasive temperature estimation: intensity and spatial prediction. Artificial Intelligence in Medicine 43(2), 127–139 (2008)